



## DISPERSAL OF TIDAL DEBRIS IN A MILKY-WAY-SIZED DARK MATTER HALO

WAYNE NGAN<sup>1</sup>, RAYMOND G. CARLBERG<sup>1</sup>, BRANDON BOZEK<sup>2,3</sup>, ROSEMARY F. G. WYSE<sup>3</sup>,  
ALEXANDER S. SZALAY<sup>3</sup>, AND PIERO MADAU<sup>4</sup>

<sup>1</sup>Department of Astronomy and Astrophysics, University of Toronto, Toronto ON, M5S 3H4, Canada; [ngan@astro.utoronto.ca](mailto:ngan@astro.utoronto.ca)

<sup>2</sup>Department of Astronomy, The University of Texas at Austin, Austin TX, 78712, USA

<sup>3</sup>Department of Physics and Astronomy, The Johns Hopkins University, Baltimore MD, 21218, USA

<sup>4</sup>Department of Astronomy and Astrophysics, University of California, Santa Cruz CA, 95064, USA

Received 2015 June 17; accepted 2016 January 17; published 2016 February 18

### ABSTRACT

We simulate the tidal disruption of a collisionless  $N$ -body globular star cluster in a total of 300 different orbits selected to have galactocentric radii between 10 and 30 kpc in four dark matter halos: (a) a spherical halo with no subhalos, (b) a spherical halo with subhalos, (c) a realistic halo with no subhalos, and (d) a realistic halo with subhalos. This allows us to isolate and study how the halo’s (lack of) dynamical symmetry and substructures affect the dispersal of tidal debris. The realistic halos are constructed from the snapshot of the Via Lactea II simulation at redshift zero. We find that the overall halo’s symmetry disperses tidal debris to make the streams fluffier, consistent with previous studies of tidal debris of dwarf galaxies in larger orbits than ours in this study. On the other hand, subhalos in realistic potentials can locally enhance the densities along streams, making streams denser than their counterparts in smooth potentials. We show that many long and thin streams can survive in a realistic and lumpy halo for a Hubble time. This suggests that upcoming stellar surveys will likely uncover more thin streams which may contain density gaps that have been shown to be promising probes for dark matter substructures.

*Key words:* dark matter – galaxies: dwarf – galaxies: interactions – Galaxy: kinematics and dynamics

### 1. INTRODUCTION

Recent surveys have discovered dynamically cold tidal debris of many disrupted stellar systems—likely globular clusters or low mass dwarf galaxies—in the inner tens of kiloparsecs of the Milky Way (Grillmair 2010, 2014; Bonaca et al. 2012; Bernard et al. 2014; Koposov et al. 2014; Martin et al. 2014). These debris, arranged in thin streams of stars, are powerful probes for the structure of our own galaxy. In particular, cold streams are more useful than hot streams for constraining the shape of the Milky Way’s halo (see Lux et al. 2013, and references therein). Also, because of their low velocity dispersion, cold streams exhibit density variations, or “gaps,” that are caused by dark matter subhalos (Yoon et al. 2011; Carlberg 2012, 2013; Carlberg et al. 2012; Carlberg & Grillmair 2013; Ngan & Carlberg 2014; Erkal & Belokurov 2015; Ngan et al. 2015).

Many theoretical studies of tidal streams rely on idealized profiles, such as logarithmic or Navarro–Frenk–White (NFW) profiles (Navarro et al. 1997), as the dark matter halo potentials of the host galaxies. Although idealized profiles have analytic forms and are simple to compute, they result from spherical averaging of many simulations of dark matter halos (Navarro et al. 1997, 2004, 2010), and the averaging does not capture the realistic details inside the individual potentials. Furthermore, both theoretical (Dubinski & Carlberg 1991; Jing & Suto 2002; Zemp et al. 2009) and observational (Law et al. 2009; Law & Majewski 2010; Deg & Widrow 2013; Vera-Ciro & Helmi 2013) efforts concluded that Milky Way’s dark matter halo is not spherical but triaxial. Some studies model the shapes of halos by introducing triaxial parameters into the radial coordinate of the idealized profiles (e.g., Law & Majewski 2010). In this study, however, we take an even more general approach to simulate tidal streams directly in the potential of Via Lactea II (VL-2), a high-resolution dark matter

halo simulation in the  $\Lambda$ CDM cosmological context (Diemand et al. 2008), without fitting the halo to any idealized profiles.

Tidal stream simulations in the VL-2 potential was first done by Bonaca et al. (2014), where they gave VL-2 its original  $N$ -body treatment, but generated tidal streams using the Streakline method (Küpper et al. 2012). In Ngan et al. (2015) we took a different approach, where we constructed a potential model using one snapshot of VL-2, but treated the tidal streams as  $N$ -body problems. The self-consistent field (SCF) method (Hernquist & Ostriker 1992) allowed us to construct accurate potential models that are optimized for dark matter halos. We furthermore isolated the subhalos found in the VL-2 halo, so we were able to construct two models: a “smooth” VL-2 halo with no subhalos, and a “lumpy” VL-2 halo with the subhalos originally found. These two models can be used to study the effects of subhalos on tidal streams in order to shed light on the “missing satellites problem” (Klypin et al. 1999; Moore et al. 1999; Yoon et al. 2011; Ngan & Carlberg 2014; Ngan et al. 2015), and we continue to use our models for this study.

Recently, Bonaca et al. (2014), Ngan et al. (2015), Pearson et al. (2015), Fardal et al. (2015) showed that streams inside non-spherical potentials exhibit fluffy features dubbed “stream-fanning” which are not found in streams inside spherical potentials. This effect has been invoked by Sesar et al. (2016) to explain the puzzling orbit and length of the recently observed Ophiuchus stream (Bernard et al. 2014; Sesar et al. 2015). This suggests that spherical potentials are no longer suitable for modeling tidal streams. It is important to note that while stream-fanning implies a non-spherical potential, the converse is not true; not all streams inside non-spherical potentials exhibit stream-fanning. The results of our study here, as we will quantify, indicate that while streams inside a realistic potential are in general wider and more diffuse than streams inside a spherical halo, thin streams can still exist even under the influence of a realistic halo and subhalos.

The goal of this study is to investigate how dispersed tidal streams are in a realistic halo, and whether we should be optimistic that large stellar surveys in the near future will be able to uncover more cold and thin streams similar to Pal-5 (Odenkirchen et al. 2001) or GD-1 (Grillmair & DiAntonio 2006). We simulate a total of 300 tidal streams as self-gravitating  $N$ -body simulations of the same globular star cluster orbiting inside the following cases of host halos: (a) a spherical halo with no subhalos, (b) a spherical halo with subhalos, (c) the VL-2 halo with no subhalos, and (d) the VL-2 halo with subhalos. In all cases, the host's and subhalos' potentials are not evolving in time, although subhalos orbit around the host's potential as test masses. Bonaca et al. (2014) fitted the VL-2's potential at different times to triaxial idealized profiles while allowing each parameter to vary radially, and they found that each parameter changed by no more than  $\lesssim 10\%$  over the last 6 Gyr. Using a time dependent potential, especially at the early stages of the halos' formation, is an important step in the future, but we believe that the effects of a realistic potential itself is worth studying before including the additional complication of time dependence.

This paper is organized as follows. Section 2 is the method section which contains several subsections. Section 2.1 summarizes the SCF method to obtain the potential from the VL-2 halo and subhalos. Section 2.2 describes our spherical halo which will be compared against the VL-2 halo. Section 2.3 justifies the mass range of subhalos included in the lumpy halo cases. Section 2.4 describes the initialization of the stream progenitor, including its density profile and its orbits. Section 3 contains our results. In particular, Sections 3.1 and 3.2 compare the dispersal of tidal debris in the spherical and the VL-2 halos, and Sections 3.3 and 3.4 discuss the effects of subhalos and how they enhance instead of lower the densities of streams. Section 4 summarizes our results and points to future work.

## 2. METHOD

### 2.1. VL-2 Halo and Subhalo Potentials

The smooth and lumpy VL-2 potentials are obtained using the same code detailed in Ngan et al. (2015), which uses a combination of the SCF method (Hernquist & Ostriker 1992) and a halo finder code to construct the gravitational potentials inside the host halo and subhalos. The  $N$ -body simulations of the streams are run using the public version<sup>5</sup> of GADGET-2 (Springel 2005). The accelerations due to both the host halo and subhalos are added to the stream particles after their  $N$ -body forces have been computed. We impose a maximum time step of 1 Myr and softening of 5 pc in each particle.

The SCF method has also been applied by Lowing et al. (2011) for the dark matter halos in the Aquarius simulations (Springel et al. 2008). In this section we briefly summarize the method, which begins by specifying a set of basis functions  $\Phi_{nlm}(\mathbf{r})$  and solves the Poisson equation in spherical coordinates  $\mathbf{r} \equiv (r, \theta, \phi)$  for the potential in the form

$$\Phi(\mathbf{r}) = \sum_{n=0}^{n_{\max}} \sum_{l=0}^{l_{\max}} \sum_{m=0}^l A_{nlm} \Phi_{nlm}(\mathbf{r}). \quad (1)$$

Given a list of particle positions and masses stored in an existing snapshot of a dark matter halo simulation, the SCF method provides a recipe to obtain the basis coefficients  $A_{nlm}$ ,

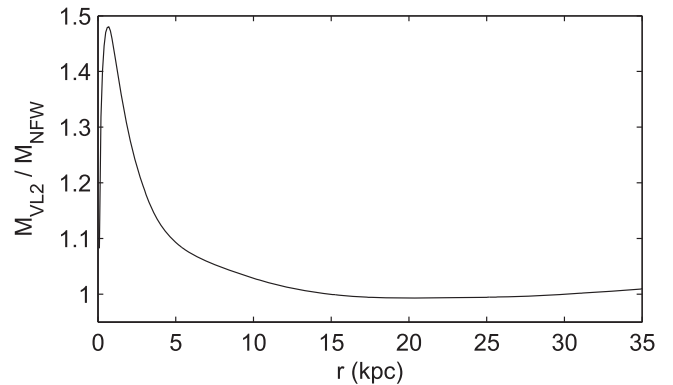


**Figure 1.** Enclosed masses of the two smooth halos used in this study. The mass of the VL-2 is computed by directly summing the masses of all the particles inside  $r$ , and the mass of the spherical halo is obtained analytically from the NFW profile. Their masses agree to within a few percent for  $10 \text{ kpc} < r < 30 \text{ kpc}$ , where our streams are selected to orbit in.

and then the force field  $-\nabla\Phi$  can be computed analytically by differentiating Equation (1). In this study, following Lowing et al. (2011) and Ngan et al. (2015), the zeroth order basis function is in the form of a Hernquist profile (Hernquist 1990), and the higher order radial and angular deviations are polynomials in  $r$  of degree  $n$  and spherical harmonics in  $(\theta, \phi)$  of orders  $l$  and  $m$ .

The smooth VL-2 potential is obtained by the SCF method using order 10 (where  $n_{\max} = l_{\max} = \text{order}$ ) on the VL-2 main halo after its subhalo particles have been removed. This order ensures that the overall shape of the main halo is captured without the lumpiness due to either the presence of subhalos or the voids after the subhalos are removed, since a polynomial of degree 10 is not sufficient to model more than 10,000 subhalos. As documented in Ngan et al. (2015), the decomposition of the main halo is performed inside the Virial radius (as reported by the halo finder), which is 400 kpc. When using an order 10 polynomial to decompose the main halo, we are only capturing features of  $\sim 40$  kpc in size. The scale radius of the largest subhalo in VL-2 is 6.4 kpc. Therefore, an order 10 polynomial for the main halo would not be sensitive to either the presence or absence of subhalos. The details for subhalo abundance are discussed in Section 2.3.

### 2.2. Spherical Halo Potential

The spherical halo is modeled using a NFW profile (Navarro et al. 1997) whose enclosed mass profile is

$$M(r) = \frac{v_h^2 r_h}{G} \left[ \ln \left( 1 + \frac{r}{r_h} \right) - \frac{r/r_h}{1 + r/r_h} \right] \quad (2)$$

where  $r_h$  and  $v_h$  are the scale parameters. We perform a least-squares fit to the VL-2 halo's mass profile at redshift zero using the NFW profile as a model. Because our streams in this study are restricted inside  $10 \text{ kpc} < r < 30 \text{ kpc}$  of the halo, as we show in Section 2.4, the fit is performed for that region only. Our best fit  $r_h$  and  $v_h$  are 19.1 kpc and  $421 \text{ km s}^{-1}$ . This gives circular velocities of 162 and  $194 \text{ km s}^{-1}$  at  $r = 10$  and 30 kpc, respectively.

Figure 1 shows the ratio of the enclosed mass profiles for our VL-2 to spherical halos. Between 10 and 30 kpc, the mass profiles agree to within a few percent. However, at less than

<sup>5</sup> <http://www.mpa-garching.mpg.de/gadget/>

10 kpc the mass profiles deviate by almost 50%. This is not surprising, as it has already been shown that VL-2's profile has an inner slope of  $\gamma = 1.24$  (Diemand et al. 2008) versus  $\gamma = 1$  in an NFW profile. Therefore, it is impossible to fit both the inner and the outer parts of the halo simultaneously. Despite this, we use the NFW profile for the spherical halo because of its simplicity and popularity in the literature. For the rest of our study, we focus on streams which only attain orbits between 10 to 30 kpc in order to facilitate a fair comparison between VL-2 and spherical halos. This is discussed in detail in Section 2.4.

The matching halo mass profiles, at least for  $10 \text{ kpc} < r < 30 \text{ kpc}$ , ensures that the dimensionless tidal scales are comparable between the two types of halos for the same star cluster mass and similar orbits. The dimensionless tidal scale  $s$ , which is the ratio between the star cluster's tidal radius and its orbital perigalacticon radius, can also be written as

$$s \equiv \left( \frac{m}{M(r)} \right)^{1/3}, \quad (3)$$

where  $m$  is the star cluster mass, and  $M(r)$  is the mass enclosed inside radius  $r$  of the host halo. Johnston (1998) and Johnston et al. (2001) found that in a spherical potential,  $s$  determines the spreads in energy and angular momentum, which in turn determine the width and length of a stream. Our goal is to study the difference between two identically distributed ensembles of streams in the VL-2 halo and a spherical halo with similar tidal scales.

### 2.3. Subhalo Finding

The lumpy host halos are simply the smooth host halos with extra subhalos orbiting in them. The subhalos of the host halos are identified and extracted from the zero redshift snapshot of VL-2 using the AMIGA HALO FINDER.<sup>6</sup> Inside the main halo of VL-2, we consider only the subhalos which are the immediate satellites of the main halo, such that all the satellites of a given subhalo (including all the hierarchically smaller satellites) are all considered as part of that subhalo.

For each subhalo, the halo finder returns the positions and velocities which are used to initialize the subhalo's orbit around the main halo, as well as masses and scale radii which are used to construct the subhalo's potential using the SCF method as described above, but with  $n_{\text{max}} = 4$  and  $l_{\text{max}} = 0$ . To ensure a fair comparison, all the subhalos in both the VL-2 and spherical host halos are modeled identically, and their orbits are initialized identically as well. The subhalos are assumed not to interact with each other and orbit the host halos as test masses, and they use the positions and velocities at redshift zero of VL-2 as orbital initial conditions.

We identify 11,523 subhalos in total whose masses range from  $6.2 \times 10^5 M_{\odot}$  to  $4.7 \times 10^9 M_{\odot}$  in the main halo in the zero redshift snapshot of VL-2. This is consistent with the abundance reported by Diemand et al. (2008). In each lumpy case, we further consider two sub-cases with two different mass ranges  $M_{\text{sub}}$  of subhalos: (i) all subhalos with  $M_{\text{sub}} > 10^7 M_{\odot}$  and (ii) all subhalos with  $M_{\text{sub}} > 5 \times 10^6 M_{\odot}$ . Our halo finder reports totals of 1087 and 2007 subhalos for the two mass ranges, respectively. These lower limits in our mass ranges are chosen such that their contributions to the dispersal of tidal

debris become significant. As we show in our results later, expanding the range of subhalos from (i) to (ii) has a negligible effect on tidal debris; meanwhile, Ngan & Carlberg (2014) showed that the inclusion of  $M_{\text{sub}} < 10^8 M_{\odot}$  subhalos can open up large gaps, which may significantly affect the distribution of debris along the stream. As opposed to Ngan & Carlberg (2014) and Ngan et al. (2015), here we do not impose an upper limit for subhalo masses because our goal is to investigate the global perturbations on tidal streams where many stars in the stream are affected (i.e., how dispersed the debris is), rather than local perturbations which only affect small parts (i.e., gaps) of the stream. Note that this means the subhalo with the highest mass in this study is more massive than those in Ngan & Carlberg (2014) and Ngan et al. (2015) which were limited to  $M_{\text{sub}} < 10^8 M_{\odot}$ .

Similar to Ngan & Carlberg (2014) and Ngan et al. (2015), in our actual simulations we do not include the subhalos which interact minimally with the streams, as some subhalos have pericentric distances that are greater than the streams' apocentric distances. As explained below, our stream orbits are restricted to a maximum apocentric distance of 30 kpc. Therefore, subhalos with pericentric distances greater than 40 kpc can be safely eliminated. For the mass ranges of subhalos mentioned above, only 381 and 674 subhalos, respectively, remain for the VL-2 potential, and 306 and 547 subhalos, respectively, remain for the spherical potential. The subhalos in both the VL-2 and spherical halos spend medians of  $\sim 0.4$  Gyr in total (out of 10 Gyr which is the duration of each stream simulation) in the inner 40 kpc of their respective halos. Since we include more subhalos in the VL-2 halo than in the spherical halo, subhalos are more likely to impact our streams in the former case. However, this does not affect our conclusions at the end.

Because the lumpy halos are essentially the smooth halos with extra subhalos, lumpy halos are more massive than smooth halos. In the VL-2 halo, 381 and 674 subhalos are about 1.6% and 1.7% of the mass of the smooth halo enclosed in its Virial radius 400 kpc. In the spherical halo, 306 and 547 subhalos are about 1.2% and 1.3% of the total mass of the smooth halo truncated at 400 kpc. In Ngan & Carlberg (2014) and Ngan et al. (2015), stream progenitors with the same initial conditions travel in roughly the same orbit in both smooth and lumpy halos because each subhalo's mass is low enough that each subhalo individually does not affect the streams' orbits much. In this study, however, stream progenitors travel in very different orbits in smooth and lumpy potentials because most of the subhalo masses are concentrated in the most massive subhalos, which can affect the streams' orbits. As shown in Yoon et al. (2011), the characteristic energy that a  $\sim 10^9 M_{\odot}$  subhalo deposits into a stream is  $\sim 10^4 \text{ km}^2 \text{ s}^{-2}$ , and this corresponds to the orbital energy  $E \propto v_{\text{orbit}}^2 \sim (200 \text{ km s}^{-1})^2$  of a GD-1-like stream whose orbit oscillates radially between 15–30 kpc. Therefore, subhalos more massive than  $\sim 10^9 M_{\odot}$  can significantly affect the orbit of the stream progenitor, hence the entire stream itself. This is the reason the smooth and lumpy halos cannot be compared directly using individual streams in each case when simulations include high mass subhalos. Smooth and lumpy halos can only be compared by the statistics of ensembles of streams as we discuss in our results in Section 3.

<sup>6</sup> <http://popia.ft.uam.es/AHF/Download.html>

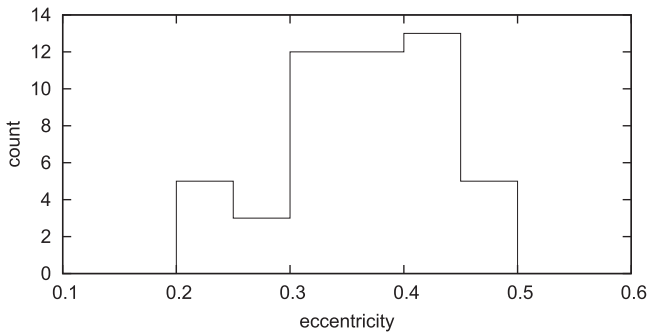


**Figure 2.** Eccentricities of the random orbits of the 50 streams simulated in each halo potential. These orbits are all selected such that their galactocentric distances  $r$  are bounded by  $10 \text{ kpc} < r < 30 \text{ kpc}$  for 10 Gyr without subhalos. This range is similar to the orbits of observed streams such as Pal-5 and GD-1 which are thin and rich in substructures. The sets of orbits in the VL-2 and spherical potentials are different, but they have identical eccentricity distribution.

#### 2.4. Stream Progenitor and Orbits

The progenitor for all streams in this study is the same self-gravitating  $N$ -body star cluster of  $N = 50,000$  particles following a King profile with  $w = 2$ , where  $w$  is the ratio between the central potential and velocity dispersion of the cluster. We initialize the cluster with core radius  $r_0 = 0.05 \text{ kpc}$  and mass  $m = 5 \times 10^4 M_\odot$ , and this yields a cluster with tidal radius  $\sim 0.15 \text{ kpc}$  (beyond which the density is zero) and velocity dispersion  $\sim 1 \text{ km s}^{-1}$ . This star cluster is typically dissolved in a few gigayears and produces a thin stream similar to GD-1 in our orbits described below.

The random orbits in our simulations are selected as follows. We first place 10,000 random points following a uniform distribution inside a spherical shell between 15 and 30 kpc in radius. Each point is also assigned uniformly random velocities between  $-300$  and  $300 \text{ km s}^{-1}$  for each of the  $v_x, v_y, v_z$  components. We then use these positions and velocities as initial conditions to integrate 10,000 test particle orbits for 10 Gyr inside both smooth VL-2 and spherical potentials.

In the VL-2 potential, we randomly select 50 orbits such that their galactocentric distances  $r$  are bounded by  $10 \text{ kpc} < r < 30 \text{ kpc}$  for 10 Gyr. The resulting eccentricity distribution of these 50 orbits selected from this process is shown in Figure 2. Here eccentricity is defined as

$$e = \frac{r_{\max} - r_{\min}}{r_{\max} + r_{\min}} \quad (4)$$

where  $r_{\max}$  and  $r_{\min}$  are the maximum and minimum  $r$  attained by the test particle in 10 Gyr. The initial conditions of these 50 orbits serve as the stream progenitor’s initial conditions for the streams’ orbits inside both smooth and lumpy VL-2 potentials.

In the spherical potential, we repeat a similar process which also selects 50 orbits with the same limiting  $r$ . However, to ensure a fair comparison, the orbits are selected such that they produce identical eccentricity distribution, shown in Figure 2, as the VL-2 case. Similarly, these 50 orbital initial conditions are applied to the stream progenitors for the streams inside both the smooth and lumpy spherical potentials.

Note that a star cluster with a density profile and orbits described above is typically dissolved after  $\sim 5 \text{ Gyr}$ , as shown in Figure 3. This ensures that computational efforts are well spent, especially because each individual stream is a fully self-gravitating simulation. Our goal is to study the dynamical

evolution of tidal tails and not the progenitors, so  $N$ -body particles that remain bound to the progenitors are irrelevant to our study. We have repeated our simulations with a more tightly bound progenitor with the same mass and tidal radius. We find that although the resulting streams are represented with fewer particles, our results are almost identical to the ones produced using the progenitor described above, which we will adopt for the rest of our results.

Also demonstrated in Figure 3 is that, for the same type of host halo and orbits, the median mass loss in smooth and lumpy halos are almost the same. In the VL-2 halo, subhalos can help dissolve the progenitor in the outlier cases, but typically this effect is very small. This means that mass loss due to subhalo shocking on the progenitor is rare, and that the orbits of the particles that are bound to the progenitor should be irrelevant. Therefore, rather than treating the progenitor and stream as an  $N$ -body system, “shortcut” methods (e.g., Küpper et al. 2012; Bonaca et al. 2014; Gibbons et al. 2014; Fardal et al. 2015) which eject test particles at the progenitor’s Lagrange points are promising alternatives. These methods potentially allow realistic streams to be generated quickly, so they are worth adopting in the future.

### 3. RESULTS

#### 3.1. Effects of the Underlying Halo

Figures 4 and 5 show the sky projections of 50 streams in each panel at 6 Gyr, as seen from the galactic center, combined into the same images for the four cases of interest in this study. The top panels of the each figure show that the dynamical symmetry of the smooth halo plays an important role in affecting the dispersal of the tidal debris. A spherical potential has four isolating integrals of motion—energy and three components of angular momentum—which constrain the phase space of the stream particles into only two dimensions (for parts of the stream that are far away from the progenitor). On the contrary, the lack of symmetry, hence the reduced number of integrals of motion, in the VL-2 halo allows the stream particles to explore the phase space with fewer constraints than when the potential is spherical. This is why the stream particles in the VL-2 halo can have a wider variety of orbits, and the streams are more diffuse than in a spherical halo.

Comparing the top and bottom panels in each of Figures 4 and 5 show that subhalos do not disperse streams as much as the lack of dynamical symmetries of the underlying halo do. This finding is similar to the conclusion from Siegal-Gaskins & Valluri (2008) which simulated the disruption of satellite galaxies that were much more massive and orbited at larger galactocentric radii (i.e., larger  $s$  from Equation (3)) than our streams. In this study we simulate the disruptions of a low mass globular cluster orbiting at smaller galactocentric radii, which result in streams that can be  $\lesssim 1^\circ$  wide as seen from the galactic center.

The right panels of Figure 5 show another interesting result. Even though the streams in the VL-2 halos are more diffuse than in the spherical halos, many of these streams remain very thin in the VL-2 halos. This is true even in the presence of subhalos which serve as time-dependent fluctuations for the streams. Therefore, thin globular cluster streams on moderately eccentric orbits (up to  $e \leq 0.5$ ) are reasonably robust against the lack of dynamical symmetry in the halo, and stellar surveys in the future will likely uncover more thin streams if they exist.

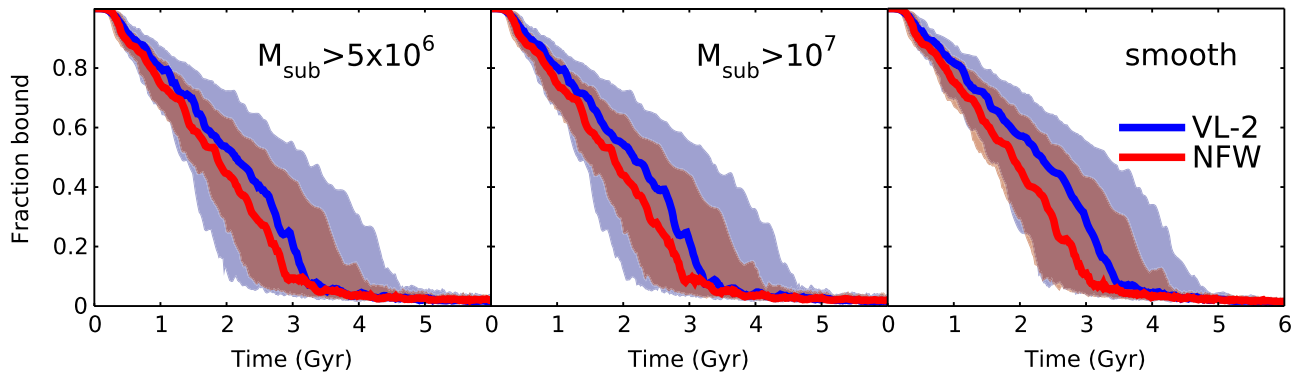


**Figure 3.** Fractions of particles enclosed in a radius 0.16 kpc of the progenitors as functions of time. Each solid line represents the median of 50 streams at each instant of time, and the colored areas enclose the points between the 15th and the 85th percentiles ( $\sim 1\sigma$ ) of the distribution at each instant of time. Each panel shows the mass range of subhalos  $M_{\text{sub}}$  present in the simulations, as labeled in units of solar masses. The similarity between these panels shows that the mass loss is primarily caused by the tidal stripping at the progenitors’ pericentric approaches, and not by subhalo shocking.

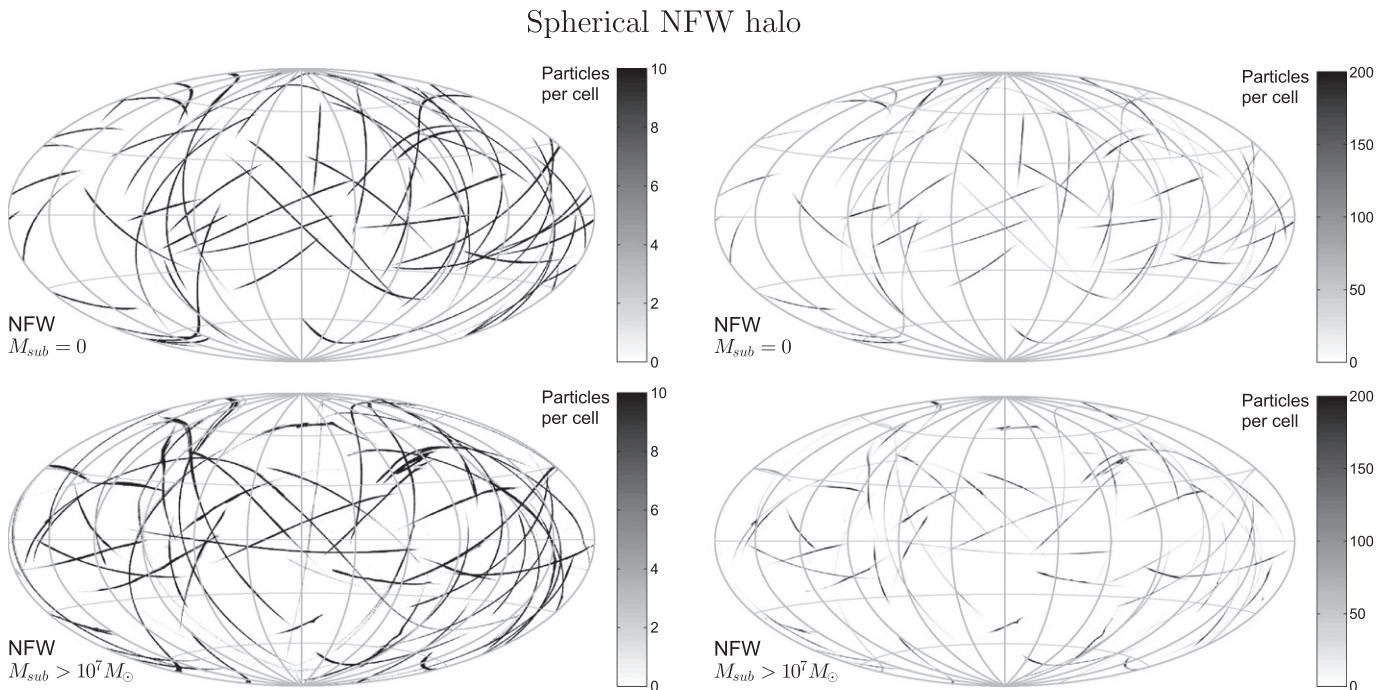


**Figure 4.** Hammer-Aitoff equal-area projections of 50 streams on the sky at 6 Gyr as seen from the galactic center. Each panel shows the combined surface density of particles in  $0.3 \times 0.3$  cells. Top and bottom rows show the streams in a smooth spherical halo and a lumpy spherical halo with  $M_{\text{sub}} > 10^7 M_{\odot}$ , respectively. Left and right columns show the same maps, but their gray scales are adjusted to emphasize the diffuse and dense cells, respectively. All orbits of the stream progenitors are selected to have their galactocentric distances  $r$  bounded by  $10 \text{ kpc} < r < 30 \text{ kpc}$  (see text for details). The orbital initial conditions of the streams are the same in top and bottom panels, but the streams travel in different orbits due to the influence of the subhalos. The case where  $M_{\text{sub}} > 5 \times 10^6 M_{\odot}$ , not shown here, produces almost identical maps to the bottom panels.

Figures 4 and 5 show the progress over the past decade or so in simulating the influence that CDM subhalos have on globular cluster streams. Pioneering studies such as Ibata et al. (2002) and Yoon et al. (2011) simulated streams inside spherical halos (though the former included a disk) in order to investigate how subhalos heat up and create gaps in streams, respectively. In addition to subsequent studies such as Carlberg (2012, 2013), Ngan & Carlberg (2014), Erkal & Belokurov (2015) which use spherical halos, the streams in the above studies would be analogous to the ones shown in Figure 4 here. In Ibata et al. (2002) they also used a flattened but still idealized potential, and the resulting streams would be an intermediate between Figures 4 and 5. It was only recently when Bonaca et al. (2014) and Ngan et al. (2015) simulated streams inside the potential of the high-resolution halo of VL-2 directly,

without fitting the potential to any idealized profiles. Their results would be analogous to the streams shown in Figure 5. It is also worth mentioning that Johnston et al. (2002), Mayer et al. (2002), Siegal-Gaskins & Valluri (2008) also simulated streams with and without subhalos, in a variety of profiles and shapes for the halo potential, but their streams were meant to be debris from dwarf galaxies and were much wider than the streams shown in Figures 4 and 5.

### 3.2. Dispersal of Tidal Debris

We now present an empirical analysis of the streams in the four cases of halos of interest. For each stream, each particle is assigned into its nearest rectangular grid cell by its three-dimensional position. The occupancies  $\eta$  of the grid cells are

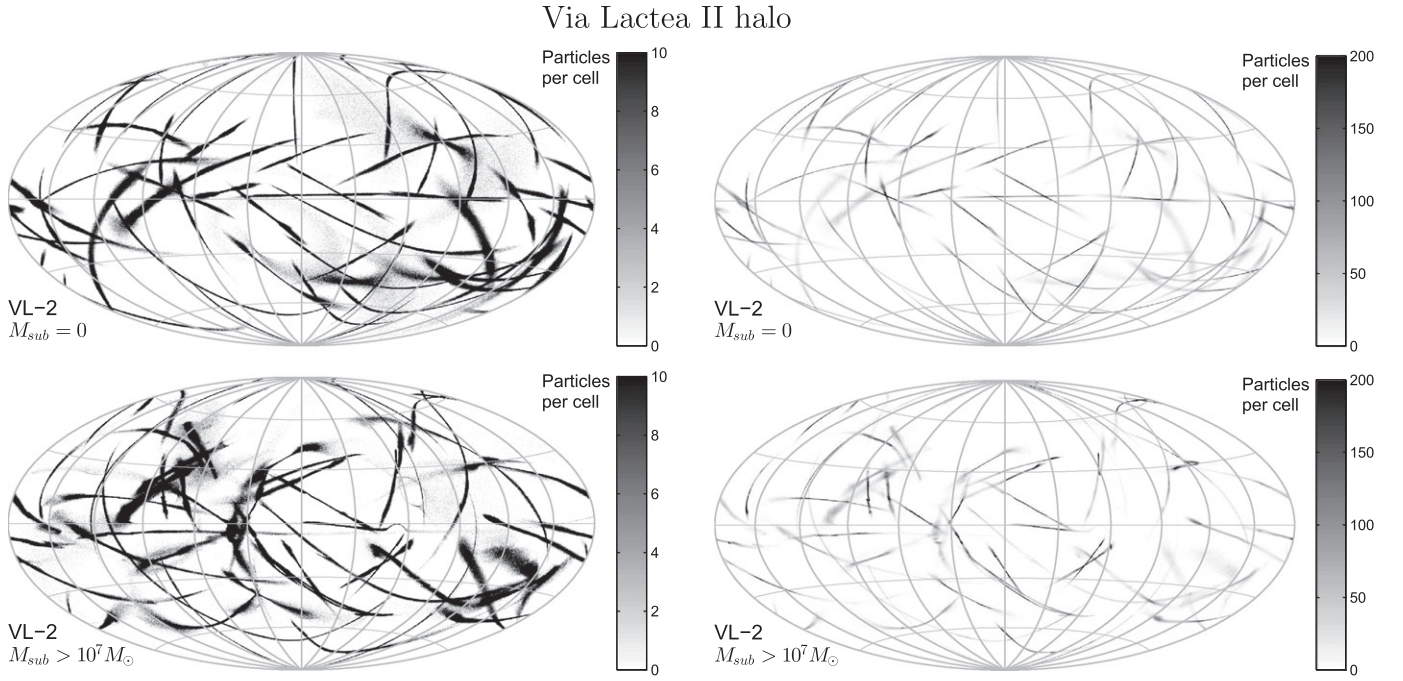


**Figure 5.** Similar to Figure 4, but the underlying halo is the VL-2 halo at redshift zero. Compared to the spherical halo in Figure 4, the streams in the VL-2 halo appear much more dispersed, especially in smooth halo (top panels). Nevertheless, some streams in the lumpy halo can also be denser than the streams in the smooth halo (see Figure 6). The orbits of the streams in this figure are selected by the same criteria and result in the same eccentricity distribution as the orbits in Figure 4.

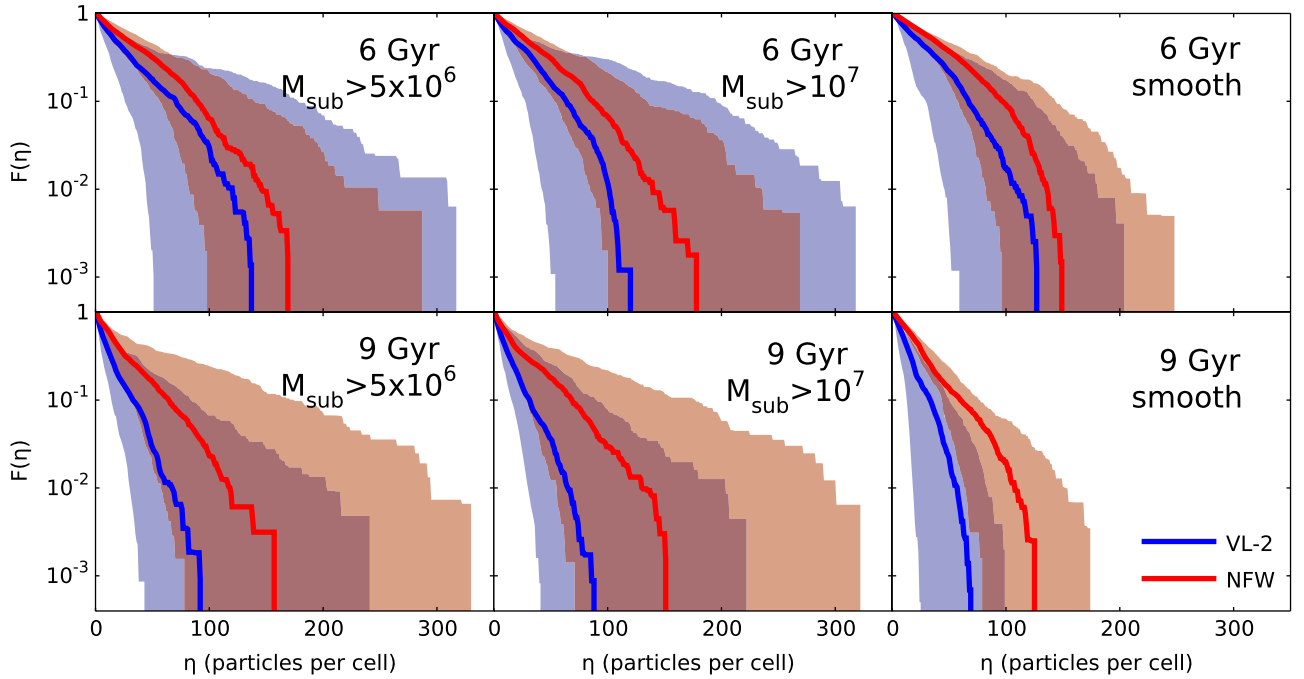


**Figure 6.** Cumulative fractions of the streams as functions of cell occupancy ( $\eta$ ) in the VL-2 and the spherical NFW halos. The solid lines are the medians of 50 streams in each case. The colored areas enclose the points between the 15th and the 85th percentiles of the distribution ( $\sim 1\sigma$ ). Top and bottom rows show the distributions at 6 and 9 Gyr, respectively. Left, middle, and right panels show the mass range of subhalos  $M_{\text{sub}}$  present in the simulations, as labeled in units of solar masses.

similar to the number densities of the streams, but we caution that our grid cells with 0.1 kpc on each side may be too coarse to be interpreted as measurements of density. This grid size is similar to the transverse full-width-half-maximum width of GD-1 at 70 pc wide (Grillmair & Dionatos 2006; Carlberg & Grillmair 2013), which is considered a very narrow stream with a derived orbit (peri- and apocenters at 14 and 29 kpc; Willett

et al. 2009) similar to orbits for our set of streams in this study. Our grid size is chosen so that it is sensitive to the particles that have been dispersed away from the main track of the stream by more than that distance.

Note that even though the densities of streams with different orbits cannot be compared directly, distributions of the cell occupancies  $f(\eta)$  can tell us how dispersed each stream is. If a

stream remains narrow without much dispersal, the occupancy of the grid would be dominated by a few densely occupied cells. On the contrary, if a stream is very dispersed, then the occupancy of the grid would be spread among many sparsely occupied cells.

Figure 6 shows the medians and the spreads of the cumulative distributions of cell occupancies of 50 streams in each of our halo potentials. The cumulative distributions have been weighted by the occupancies and then normalized by the total numbers of particles. More precisely, the  $y$ -axes are

$$F(\eta) = \frac{1}{N} \sum_{k>\eta} kf(k) \quad (5)$$

where  $N = 50,000$  is the total number of particles in each stream. So,  $F(\eta)$  can be thought of as the fraction of the stream such that the cell occupancy is higher than  $\eta$ .

At early times when the streams are  $\lesssim 5$  Gyr old, due to their moderate orbital eccentricities the streams did not have time to develop extended tails. Furthermore, Figure 3 shows that at  $\lesssim 5$  Gyr some stream progenitors are still on the verge of being completely dissolved. For these streams, their occupancy distributions would be dominated by the final remnants of the progenitors, which are trivially the densest points in each stream. For these reasons, in Figure 6 we show only the occupancy distributions at later times such as 6 and 9 Gyr.

Figure 6 is essentially the quantification of Figures 4 and 5. Recall that those two figures clearly show that the streams in the VL-2 halo are much more diffuse than the streams in the spherical halo, with or without subhalos in each case. This is quantified in Figure 6, where the streams in the VL-2 halo (blue line and regions) consistently have lower  $\eta$  than the streams in the spherical halo (red line and regions) in every panel. At the diffuse end ( $\eta \lesssim 100$  particles per cell), the fractions of the streams can differ by as much as two orders of magnitude between streams in the two types of halos. As discussed above, this can be attributed to the wider variety of orbits that the VL-2 halo permits due to its lack of dynamical symmetry. In particular, extremely “fluffy” streams can be found in Figure 5 and have been investigated in more detail by Ngan et al. (2015), Pearson et al. (2015), Price-Whelan et al. (2016).

### 3.3. Effects of Subhalos

The tools developed in the previous section allow us to quantify how subhalos disperse tidal debris, which is difficult to see by eye in Figures 4 and 5. The effects of subhalos are shown in the left and middle columns of Figure 6. First of all, those two columns have negligible differences. This means that subhalos with masses below  $10^7 M_\odot$  do not contribute significantly to dispersing tidal debris. Indeed, versions of Figures 4 and 5 with  $M_{\text{sub}} > 5 \times 10^6 M_\odot$  (not shown here) look almost identical to Figures 4 and 5 with  $M_{\text{sub}} > 10^7 M_\odot$ . For the rest of our results, the “lumpy halo” refers to the case of a halo with the subhalo mass range  $M_{\text{sub}} > 10^7 M_\odot$ .

Nevertheless, subhalos of masses  $M_{\text{sub}} < 10^7 M_\odot$  do inject enough energy to disperse tidal debris and produce gaps in tidal streams. However, as shown in Yoon et al. (2011), the change in energy of the debris decrease rapidly with distance from the impact, and the rate of this decrease depends on the subhalo’s mass. More massive subhalos can inject energy at parts of the stream farther away from the impact, whereas less massive subhalos can only do so locally. In other words, the “gaps”

produced by  $M_{\text{sub}} > 10^7 M_\odot$  subhalos are big enough that they may affect large parts of the streams. Our results here focus on the effects of these massive subhalos.

A surprising feature can be seen when we compare streams in the smooth and the lumpy halos of the same halo type (i.e., same colors between middle and right columns of Figure 6). Intuitively, one may think that subhalos can scatter stars away from a stream’s path, and this would decrease the  $\eta$  of the stream. However, upon closer inspection of Figure 6, some streams in lumpy halos can behave in the opposite manner. At the diffuse end,  $F(\eta)$  for the streams in lumpy halos are no lower than those in smooth halos. At the dense end,  $F(\eta)$  for the streams in lumpy halos are consistently much higher than those in smooth halos. Therefore, while the reduction of dynamical symmetry in the halo can make streams more diffuse, the lumpiness of the halo can make certain parts of streams denser. In the next section, we investigate how the densities in these streams are enhanced.

Density enhancements due to the lumpiness of the halo has important implication for stellar surveys in the near future. The streams that are denser have higher surface brightness, so they may be more easily found in surveys. This means that if the  $\Lambda$ CDM prediction of the lumpiness of the Milky Way’s halo is true, then globular cluster streams should be easier to detect. This is a very encouraging result because the detailed structures along these streams, in turn, contain crucial information about the  $\Lambda$ CDM prediction itself (see references in Section 1).

### 3.4. The Densest Streams in the VL-2 Halos

In this section we investigate the streams which orbit the VL-2 halo and contain the densest parts compared to other streams. In order to avoid identifying the stream progenitors as trivially the densest parts of the streams, we only investigate streams at 9 Gyr to ensure that all streams are completely dissolved (except one stream whose progenitor actually survived for 10 Gyr. This stream is not being considered for the rest of this section). We follow our analysis in the previous section where we assign the particles of each stream into a 3D grid with cell size of 0.1 kpc on each side. For each stream we consider the cell with the maximum occupancy  $\eta_{\text{max}}$ , and we sort the streams by their  $\eta_{\text{max}}$ . The sky projections and  $F(\eta)$  plots of six streams which contain the highest  $\eta_{\text{max}}$  are shown in Figures 7 and 8. Note that these streams rank above the 85th percentile at the densest end of the stream distributions, so the lines in Figure 8 lie well outside of the blue regions in the bottom panels of Figure 6.

In the smooth VL-2 halo the densest streams are  $\lesssim 1^\circ$  thin as seen from the galactic center. In Figure 7 stream A is compressed transversely as it undergoes a pericentric passage, but stream B has just gone past an apocentric passage. This means that without subhalos, not only can thin globular streams survive in a realistic halo for a Hubble time, but they are also the densest and easiest to find regardless of their orbital phases.

In the lumpy VL-2 halo, not only are the streams with the highest  $\eta_{\text{max}}$  long and  $\lesssim 1^\circ$  thin similar to those in the smooth halo, but careful inspection of Streams C, D, E, and F in Figure 7 also reveals density variations along them. Density variation in one stream in the VL-2 halo has previously been reported in Ngan et al. (2015) but with a different subhalo mass range. Our study here shows that even in the presence of subhalos more massive than those ( $10^8 M_\odot$ ) included in Ngan et al. (2015), many streams remain thin for a Hubble time.

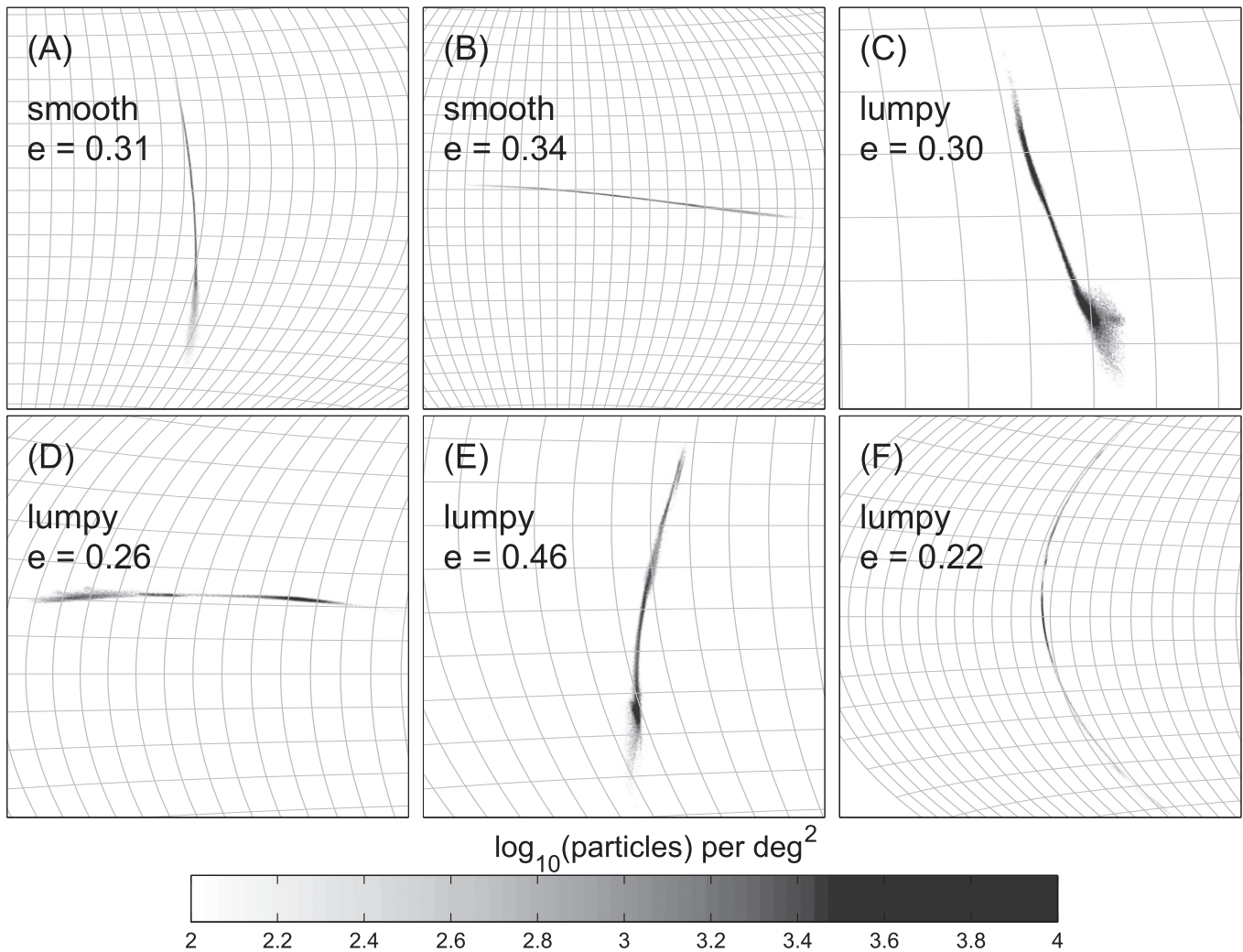


**Figure 7.** Six of the densest streams at 9 Gyr in the VL-2 halo. Each stream is projected onto the sky using Hammer-Aitoff equal-area projection as seen from the galactic center. Both latitudinal and longitudinal grid lines in all panels are spaced at  $5^\circ$  apart. The lumpy halo for streams C, D, E, and F contains subhalos at  $M_{\text{sub}} > 10^7 M_\odot$ . Eccentricities  $e$  for the streams in the lumpy halo are quoted for the streams’ orbits without subhalos. Note that the color scale is the log of the number of particles in each bin at  $0.1$  on each side. In the smooth halo, stream A is undergoing a pericentric passage, but stream B is not. In the lumpy halo, the streams which contain the densest points are also thin, but the densest points are clumps that were caused by interactions with subhalos.

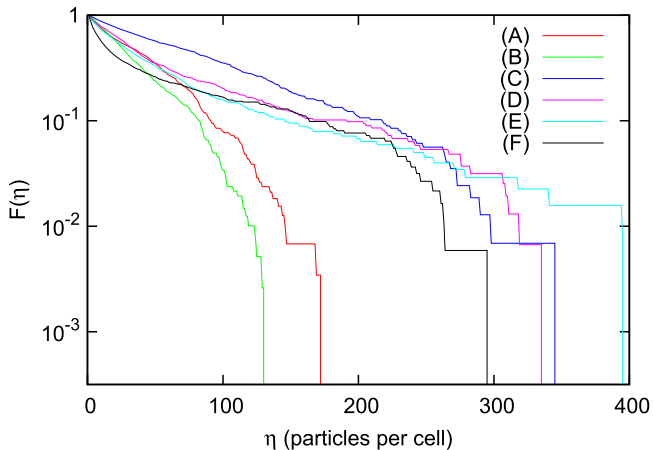


**Figure 8.** Cumulative distribution  $F(\eta)$  of cell occupancy for the six streams shown in Figure 7. Streams A and B are in the smooth VL-2 halo, and streams C, D, E, and F are in the lumpy VL-2 halo. These streams are outliers of the dense end in the distributions shown in blue in the bottom panels of Figure 6.

The densest point of all the streams shown in Figure 7 is the clump at the lower tip of Stream E, whose  $\eta$  distribution is shown as the light blue line in Figure 8. That clump originated from a direct impact by a subhalo with mass  $M_{\text{sub}} = 1.0 \times 10^8 M_\odot$  and scale radius  $r_s = 0.8$  kpc at  $\sim 6.4$  Gyr. The part of the stream which sustained the impact was moving at  $v_{\text{stream}} \simeq (107, -10, -120) \text{ km s}^{-1}$ , and the subhalo was moving at  $v_{\text{sub}} \simeq (143, 378, -88) \text{ km s}^{-1}$ . Shortly after the impact at 6.46 Gyr (upper left panel of Figure 9), a density minimum can be seen at the point of impact in between two density peaks. This is consistent with the matched filter profiles used in Carlberg (2012) and Ngan & Carlberg (2014) to look for gaps. The stream particles at the point of impact sustained changes of energy of  $\sim 200 \text{ km}^2 \text{ s}^{-2}$ , which agrees with the analytical estimate shown in Figure 4 in Yoon et al. (2011). At later times (upper right and lower left panels) the impact causes a shift in the stream particles’ orbits, and the stream develops a “z-fold” which was seen in the idealized simulations in Carlberg (2009). As the fold evolves with the stream, both tips of the fold can overlap and occupy the same grid cells. This is seen in the lower right panel where the fold

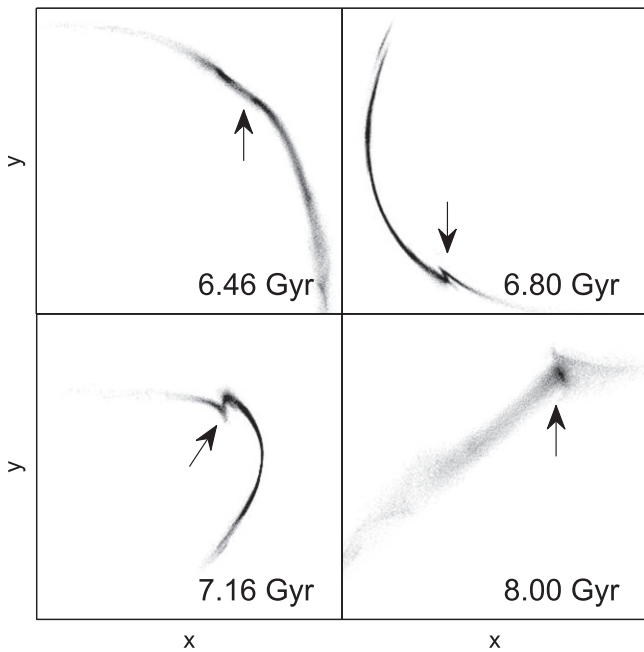


**Figure 9.** Time evolution of Stream E in Figure 7. Each panel shows the surface density of the stream projected onto the  $xy$ -plane at different times as labeled. All panels are 16 kpc on each side, and have the same color scale. The arrow indicates the position where a subhalo of  $M_{\text{sub}} = 1.0 \times 10^8 M_{\odot}$  had a direct impact the stream at 6.42 Gyr, which later became a very dense clump along the stream.

evolved into a clump by 8, or 1.6 Gyr after the impact. This is the reason that the typical  $\eta_{\text{max}}$  for streams in the lumpy halo is  $\sim 2$  times higher than in the smooth halo.

All streams D, E, and F had encounters with  $M_{\text{sub}} \gtrsim 10^8 M_{\odot}$  subhalos where the impact parameter is less than the scale radius of the subhalo. Stream C is an interesting case as it has only had one close encounter with a  $M_{\text{sub}} = 1.6 \times 10^7 M_{\odot}$  subhalo. The effect of this encounter is much less pronounced as that shown in Figure 9, but it induces density variation along the stream nonetheless. Careful inspection of Figure 8 reveals that although Stream C does not have the highest  $\eta_{\text{max}}$ , at the intermediate  $\eta \lesssim 250$  range it has the highest fraction compared to other streams. This is partially also due to its apocentric approach where the stream is longitudinally compressed at that time. This compression, together with the density variation induced by subhalos, makes Stream C one of the densest streams overall.

#### 4. CONCLUSION

In this study we investigated the dispersal of a total of 300 tidal streams which resulted from the disruption of a globular star cluster in four kinds of dark matter halos:

- (a) Spherical potential with no subhalos.
- (b) Spherical potential with orbiting subhalos.
- (c) Realistic potential with no subhalos.
- (d) Realistic potential with orbiting subhalos.

Both cases with subhalos (b) and (d) were further divided into two sub-cases with different subhalo mass ranges: (i) all subhalos with  $M_{\text{sub}} > 10^7 M_{\odot}$ , and (ii) all subhalos with  $M_{\text{sub}} > 5 \times 10^6 M_{\odot}$ . In all cases the main halo was a time independent potential constructed using the zero redshift snapshot of the high-resolution dark matter halo in the Via

Lactea II (VL-2) simulation. The subhalos were extracted by a halo finder code from VL-2 and were also constructed as time independent potentials, but they orbited around the smooth potentials.

For each case above, we simulated 50  $N$ -body streams whose progenitor orbits were inside galactocentric radii of  $10 \text{ kpc} < r < 30 \text{ kpc}$  in the smooth potentials (while allowing subhalos to scatter the tidal debris to arbitrary distances) for 10 Gyr. The stream orbits were results from randomly distributed infall velocities, and the radial range were chosen to be rough matches with well-studied globular cluster streams such as Pal-5 and GD-1.

For each stream we quantified the dispersal of the tidal debris by assigning all particles to their nearest grid cells, and we plotted the distributions of cell occupancies. We found that the lack of dynamical symmetry of the smooth halo can disperse tidal debris more than subhalos do, similar to the conclusion of Siegal-Gaskins & Valluri (2008) which simulated the tidal disruptions of dwarf galaxies in larger orbits. On the other hand, we found that subhalos with  $M_{\text{sub}} > 10^7 M_{\odot}$  can make some streams much denser, hence more easily detectable, by bunching up stream stars into clumps which were denser than streams in the smooth halo. Meanwhile, subhalos with  $M_{\text{sub}} > 5 \times 10^6 M_{\odot}$  produced almost the same distribution of cell occupancies as the  $M_{\text{sub}} > 10^7 M_{\odot}$  case. Therefore, even though subhalos with masses below  $10^7 M_{\odot}$  can produce gaps in streams as shown in previous studies, these subhalos are not important for globally redistributing the material in a stream.

We selected a few streams which produced the highest cell occupancies—hence, most easily detectable—in the VL-2 halo in order to study their morphologies. In the smooth halo, these dense streams are long and  $\lesssim 1^\circ$  thin as seen from the galactic center. This suggests that even though a realistic halo disperses tidal debris, long and thin streams can still survive for a Hubble time. In the lumpy halo, the streams with the highest cell occupancies were just as long and thin as those in the smooth halo; however, the densest parts of the streams were primarily due to subhalo perturbations which caused stream particles to bunch up. This increased the occupancies of the cells near the point where the bunch up occurred. Combined with the effect of longitudinal compression at the streams' apocentric passages, streams in a lumpy halo can be much denser than those in a smooth halo.

To put our results into context, the streams in our study were similar to (but not physical models of) globular streams such as Pal-5 and GD-1. These streams have been well modeled and studied, and are excellent sources of knowledge about the dark matter halo in our own galaxy. It would be very useful if more streams similar to them are detected in the future, should they exist. The question we sought to answer was whether the lack of dynamical symmetry of the halo potential or the lumpiness of the halo would erase these streams, thus discouraging us from searching for more. As summarized in Figures 5 and 7, our conclusion is that even though streams inside realistic cases are more dispersed, many of them can survive as long and thin structures over a Hubble time. In fact, the presence of subhalos may even make some streams easier to detect.

While our  $N$ -body streams are orbiting realistic halo potentials, our simulations are still missing a few effects. In addition to a dark matter halo, the Milky Way also has a baryonic galaxy which was not included in our study. Previous studies such as Dehnen et al. (2004) and Brooks & Zolotov

(2014 and references therein) found that the galactic disk can influence the mass loss rates of globular clusters and dwarf galaxies, respectively. However, the effect of a galactic disk on the dispersal of tidal debris has yet to be studied in detail. Furthermore, other than the subhalos' orbits, all our potentials are static since we constructed them using only the redshift zero snapshot. In the hierarchical structure formation model, satellite systems are continuously accreted and merged into the main halo. Therefore, we expect both the main halo and the subhalos to be evolving in time. Finally, we selected our stream orbits randomly in both positions and velocities, which likely resulted in an unrealistic distribution of orbits. Current surveys such as Gaia (Perryman et al. 2001) will be very valuable in providing detailed information of kinematics of globular clusters and streams in the Milky Way for future studies.

The authors thank the referee for a very detailed and constructive review. R.W., A.S., and B.B. (at JHU) are supported by NSF grant OIA-1124403, and P.M. by OIA-1124452. Computations were performed on the GPC super-computer at the SciNet HPC Consortium, as well as Sunnyvale at the Canadian Institute of Theoretical Astrophysics. SciNet is funded by: the Canada Foundation for Innovation under the auspices of Compute Canada; the Government of Ontario; Ontario Research Fund—Research Excellence; and the University of Toronto.

## REFERENCES

- Bernard, E. J., Ferguson, A. M. N., Schlafly, E. F., et al. 2014, *MNRAS*, **443**, L84
- Bonaca, A., Geha, M., & Kallivayalil, N. 2012, *ApJL*, **760**, L6
- Bonaca, A., Geha, M., Küpper, A. H. W., et al. 2014, *ApJ*, **795**, 94
- Brooks, A. M., & Zolotov, A. 2014, *ApJ*, **786**, 87
- Bullock, J. S., & Johnston, K. V. 2005, *ApJ*, **635**, 931
- Carlberg, R. G. 2009, *ApJL*, **705**, L223
- Carlberg, R. G. 2012, *ApJ*, **748**, 20
- Carlberg, R. G. 2013, *ApJ*, **775**, 90
- Carlberg, R. G., & Grillmair, C. J. 2013, *ApJ*, **768**, 171
- Carlberg, R. G., Grillmair, C. J., & Hetherington, N. 2012, *ApJ*, **760**, 75
- Deg, N., & Widrow, L. 2013, *MNRAS*, **428**, 912
- Dehnen, W., Odenkirchen, M., Grebel, E. K., & Rix, H.-W. 2004, *AJ*, **127**, 2753
- Diemand, J., Kuhlen, M., Madau, P., et al. 2008, *Natur*, **454**, 735
- Dubinski, J., & Carlberg, R. G. 1991, *ApJ*, **378**, 496
- Erkal, D., & Belokurov, V. 2015, *MNRAS*, **450**, 1136
- Fardal, M. A., Huang, S., & Weinberg, M. D. 2015, *MNRAS*, **452**, 301
- Gibbons, S. L. J., Belokurov, V., & Evans, N. W. 2014, *MNRAS*, **445**, 3788
- Grillmair, C. J. 2010, in *Galaxies and Their Masks*, ed. D. L. Block, K. C. Freeman, & I. Puerari (New York: Springer), 247
- Grillmair, C. J. 2014, *ApJL*, **790**, L10
- Grillmair, C. J., & Dionatos, O. 2006, *ApJL*, **643**, L17
- Hernquist, L. 1990, *ApJ*, **356**, 359
- Hernquist, L., & Ostriker, J. P. 1992, *ApJ*, **386**, 375
- Ibata, R. A., Lewis, G. F., Irwin, M. J., & Quinn, T. 2002, *MNRAS*, **332**, 915
- Jing, Y. P., & Suto, Y. 2002, *ApJ*, **574**, 538
- Johnston, K. V. 1998, *ApJ*, **495**, 297
- Johnston, K. V., Sackett, P. D., & Bullock, J. S. 2001, *ApJ*, **557**, 137
- Johnston, K. V., Spergel, D. N., & Haydn, C. 2002, *ApJ*, **570**, 656
- Klypin, A., Kravtsov, A. V., Valenzuela, O., & Prada, F. 1999, *ApJ*, **522**, 82
- Koposov, S. E., Irwin, M., Belokurov, V., et al. 2014, *MNRAS*, **442**, L85
- Küpper, A. H. W., Lane, R. R., & Heggie, D. C. 2012, *MNRAS*, **420**, 2700
- Law, D. R., & Majewski, S. R. 2010, *ApJ*, **714**, 229
- Law, D. R., Majewski, S. R., & Johnston, K. V. 2009, *ApJL*, **703**, L67
- Lowing, B., Jenkins, A., Eke, V., & Frenk, C. 2011, *MNRAS*, **416**, 2697
- Lux, H., Read, J. I., Lake, G., & Johnston, K. V. 2013, *MNRAS*, **436**, 2386
- Martin, N. F., Ibata, R. A., Rich, R. M., et al. 2014, *ApJ*, **787**, 19
- Mayer, L., Moore, B., Quinn, T., Governato, F., & Stadel, J. 2002, *MNRAS*, **336**, 119
- Moore, B., Ghigna, S., Governato, F., et al. 1999, *ApJL*, **524**, L19
- Navarro, J. F., Frenk, C. S., & White, S. D. M. 1997, *ApJ*, **490**, 493
- Navarro, J. F., Hayashi, E., Power, C., et al. 2004, *MNRAS*, **349**, 1039
- Navarro, J. F., Ludlow, A., Springel, V., et al. 2010, *MNRAS*, **402**, 21
- Ngan, W., Bozek, B., Carlberg, R. G., et al. 2015, *ApJ*, **803**, 75
- Ngan, W. H. W., & Carlberg, R. G. 2014, *ApJ*, **788**, 181
- Odenkirchen, M., Grebel, E. K., Rockosi, C. M., et al. 2001, *ApJL*, **548**, L165
- Pearson, S., Küpper, A. H. W., Johnston, K. V., & Price-Whelan, A. M. 2015, *ApJ*, **799**, 28
- Perryman, M. A. C., de Boer, K. S., Gilmore, G., et al. 2001, *A&A*, **369**, 339
- Price-Whelan, A. M., Johnston, K. V., Valluri, M., et al. 2016, *MNRAS*, **455**, 1079
- Sesar, B., Bovy, J., Bernard, E. J., et al. 2015, arXiv:1501.00581
- Sesar, B., Price-Whelan, A. M., Cohen, J. G., et al. 2016, *ApJL*, **816**, L4
- Siegal-Gaskins, J. M., & Valluri, M. 2008, *ApJ*, **681**, 40
- Springel, V. 2005, *MNRAS*, **364**, 1105
- Springel, V., Wang, J., Vogelsberger, M., et al. 2008, *MNRAS*, **391**, 1685
- Vera-Ciro, C., & Helmi, A. 2013, *ApJL*, **773**, L4
- Willett, B. A., Newberg, H. J., Zhang, H., Yanny, B., & Beers, T. C. 2009, *ApJ*, **697**, 207
- Yoon, J. H., Johnston, K. V., & Hogg, D. W. 2011, *ApJ*, **731**, 58
- Zemp, M., Diemand, J., Kuhlen, M., et al. 2009, *MNRAS*, **394**, 641